Article

Sustainable polypropylene-based composites with agro-waste fillers: thermal, morphological, mechanical properties, and dimensional stability.

Tatiana Zhiltsova *, Jéssica Campos , Andreia Costa , Mónica S. A. Oliveira

Posted Date: 11 December 2023

doi: 10.20944/preprints202312.0697.v1

Keywords: natural fibre-reinforced composites; olive pits; rice husk; non-destructive morphology assessment; polypropylene; short-term water absorption

Article

Sustainable Polypropylene-Based Composites with Agro-Waste Fillers: Thermal, Morphological, Mechanical Properties, and Dimensional Stability

Tatiana Zhiltsova [1,*], Jéssica Campos [2], Andreia Costa [3] and Mónica S. A. Oliveira [1]

[1] Mechanical Engineering Department, University of Aveiro, Aveiro, Portugal; TEMA—Centre for Mechanical Engineering and Automation, University of Aveiro, Aveiro, Portugal; LASI—Intelligent Systems Associate Laboratory,4800-058 Guimarães, Portugal; monica.oliveira@ua.pt

[2] Mechanical Engineering Department, University of Aveiro, Aveiro, Portugal; jessica.e.campos@ua.pt

[3] OLI-Sistemas Sanitários, S.A. Travessa de Milão, Esgueira, 3800-314 Aveiro, Portugal; andreiac@oli-world.com

* Correspondence: tvzhiltsova@ua.pt

Abstract: Natural Fibre Composites (NFC) are eco-friendly, sustainable alternatives to synthetic polymers. However, some intrinsic natural fillers´ properties hinder their widespread implementation as reinforcement in polymeric matrices and require further investigation. In the scope of this study, the thermal, rheologic, mechanical (tension and flexural modes), morphological properties, water absorption and dimensional stability of the NF polypropylene (PP) based injection moulded composites with the rice husk (rh) and olive pits (op) of 20 wt% and 30% wt%, were investigated. The results suggest that the higher content of the rice husk and olive pits led to a similar reduction of the Melt Flow Index (MFI), independent of the additive type compared to virgin polypropylene (PPv). The melting and crystallization temperatures of the PPrh and PPop composites did not change with statistical significance. The composites are stiffer than the PP matrix by up to 49% and possess higher mechanical strength in what concerns the tension mode at the expense of decreased ductility. PPrh and PPop have superior flexural modulus in the bending mode, while the flexural strength improvement was accomplished for the PP30%rh. The dimensional stability of the composites was improved as the linear shrinkage in the flow direction was decreased by 49% for PPrh and 30% for PPop, positively correlating with an increase in the filler content and stiffness. PPop was less susceptible to water sorption than PPrh due to fibres' composition and larger surface-to-area volume ratios.

Keywords: natural fibre-reinforced composites; olive pits; rice husk; non-destructive morphology assessment; polypropylene; short-term water absorption

---

The exponential growth of synthetic polymer production and consumption has resulted in severe problems related to product disposal and depletion of petrochemical feedstocks. Eco-friendly alternative polymer materials are being developed to address environmental and societal concerns. Natural Fibre Composites (NFC) have garnered substantial interest and extensive research. Such materials have improved environmental behaviour and an optimized load-bearing capacity, meeting the quality requirements of polymer components while reducing the reliance on synthetic polymers [1–4].

Agriculture is a significant economic activity in Portugal. It, however, generates a large amount of waste that needs to be disposed of properly. Every year Portugal produces about 160,000 tons of paddy rice, generating as a by-product about 20% rice husk of this amount [5]. Another important Portuguese agro-industry is olive production. In 2022, olive production in mainland Portugal amounted to 774,743 tons, which generated significant olive pit residuals after oil extraction [6]. The amount of these two industries' production makes rice husk and olive pit the most abundant agro-industrial waste products in Portugal. Regarding the disposal of these agro-residuals, until recently, the primary disposal route was energy generation through incineration, collaterally aggravating environmental pollution [7]. Compared to other agro-waste sources, these fibres are challenging to

 doi:10.20944/preprints202312.0697.v1

reutilize, making them unsuitable for animal feeding due to their lack of nutritional value. However, using them as a renewable natural fibre source for reinforcement of polymer-based composites is a more economical and environmentally friendly alternative [8–11]. These composites exhibit low density, high mechanical strength and stiffness, and effective thermal and acoustic insulation. Additionally, NFCs have a reduced environmental impact and require fewer resources during processing compared to synthetic fibres [12]. Over recent years, a vast body of literature has been dedicated to polyolefin-based NF composites reinforced with rice husk and olive pit fibres. The focus on polyolefins as a choice for polymer matrix is easy to understand due to their excellent chemical and moisture resistance, low density, good mechanical properties, low cost and capability to be industrially processed through different methods such as injection moulding and extrusion [13].

A few challenges are hindering the broad implementation of NFCs. One of the problems arises from the chemical structure of lignocellulosic fibres having several hydroxyl functional groups at the surface, which create a weak interfacial interaction with the functional group in the polymer matrix and promote moisture absorption [14]. The typical way to improve the natural filler/matrix interactions is the addition of coupling agents. Maleic anhydride grafted polyolefins are the most frequently applied coupling agents and have been investigated in many studies for polyolefin-based composites. Using coupling agents improves the adhesion quality between polymer and filler by reducing the gaps in the interfacial region, simultaneously blocking the hydrophilic groups. The impact of the maleic anhydride grafted polyolefins on the NFC quality is multifold: dimensional stability improvement [15], water absorption decrease [16,17], and mechanical properties improvement [3,15,17,18]. In addition, much research has been dedicated to precisely defining the natural filler content toward maximum improvement of the NFC mechanical properties. The common ground is an improvement of the elastic mechanical properties, i.e. higher stiffness at the expense of significant ductility loss due to the insufficient wetting of the fibres by the polymer matrix [2,3,14,19–23].
However, when very heavy natural filler loading is concerned, higher loading may not correlate with better mechanical performance [1,24].

A few studies were found dealing with the dimensional stability of NFC [15,25], and none investigating rice husk and olive pit injection moulded composites shrinkage properties, requiring further investigation on this topic. Moreover, to the authors' knowledge, no research has been reported on the non-destructive morphology assessment of injection moulded NFC, which may be essential for establishing the structure-property relationship. X-ray computed tomography (CT) analyses have been used so far for synthetic composite materials, focusing primarily on assessing the porosity and morphology of fibres [26]. To advance larger-scale industrial implementation of natural fibre composites, both dimensional stability and non-localized morphology evaluation should be addressed.

In light of the above, this study aims to establish the suitability of the industrially prepared rice husk and olive pit composites for application in functional products such as sanitary components aiming for synthetic polymer replacement, complying this way with the objectives of the project "OLIpush – Redesign for greater circularity and a smaller environmental foot-print". For this purpose, water absorption, thermal, mechanical, physical, and morphological properties of the rice husk and olive pit polypropylene composites with different combinations of fibre loading were investigated.

2. Materials and Methods

2.1. Materials

PP-based NFCs with 20 and 30% wt. of rice husk and olive pits were provided by Bio4plas - Biopolímeros, Lda. 1 wt.% of ExxonMobil EXXELOR™ PO 1020 Maleic anhydride functionalized polypropylene (PPMA) was added to the compound to improve matrix/fibre compatibility. Before compounding in a double screw extruder with degassing, rice husk and olive pits were dried until they reached approximately 0.7% humidity. The humidity level of the fibres was assessed by

Preprints (www.preprints.org) | NOT PEER-REVIEWED | Posted: 11 December 2023 doi:10.20944/preprints202312.0697.v1

gravimetric moisture measurement with a moisture balance. The rice husks and olive pits were shredded and sieved through the mesh strainer (mesh size 0.5 mm). The composition of composites and their designations, referred to through the text hereafter, are listed in Table 1. The virgin 205CA-40 - Polypropylene Random Copolymer by INEOS Olefins & Polymers Europe (PPv) was used for composites' preparation as a polymer matrix and the property's comparison.

Table 1. Materials' composition.

Designation	Composition (%)			
	PP	rice husk	olive pits	PPMA
PPv	100	-	-	-
PP20%rh	79	20	-	1
PP30%rh	69	30	-	1
PP20%op	79	-	20	1
PP30%op	69	-	3	1

2.2. Methods

2.2.1 Melt Flow Index

The measurements of the melt flow index were performed on the machine Göttfert MI-3 (GÖTTFERT Werkstoff-Prüfmaschinen GmbH, Buchen, Germany) by the standard ISO 1133-1991 (2,16 kg, 190 °C). Each NFC lot and virgin PP was analysed with five samples to ensure accuracy and reliability. Melt density was calculated as a relation between the MFI (g/10 min) and the MVR (Melt Volume Rate, cm3/10 min), as shown in Equation 1

$$\rho_m = \frac{MFI}{MVR} \quad (1)$$

2.2.2. Differential Scanning Calorimetry

For the determination of melting (Tm) and crystallisation (Tc) temperatures, as well as melting (ΔHm) and cold crystallisation (ΔHc) enthalpies, differential scanning calorimetry (DSC) was performed on samples weighing approximately 5 to 10 mg. The DSC tests were carried out using the DSC Discovery 250 instrument (TA Instruments, New Castle, DE, USA) following the standard ISO 11357-3 guidelines. TRIOS software, the proprietary software of TA Instruments, was used for data analysis. To eliminate any thermal history of the material, each material lot underwent two heating and cooling cycles. The data from the second cycle were collected and analysed. Three samples were analysed for each material lot. The DSC analysis involved stabilising each sample at 20 °C, followed by heating it up to 190 °C and then cooling it back to 20 °C at a rate of 10 °C/min. The degree of crystallinity (χ) for each sample was calculated using Equation 2 [23].

$$\chi(\%) = \frac{H_m}{H_m^0 \times f_{pp}} \times 100, \quad (2)$$

Where ΔHm (J/g) represents the melting enthalpy of the polymer under analysis, the melting enthalpy of 100% crystalline PP (ΔH0m) is known to be 207 J/g [27]. The variable fpp denotes the weight fraction of PP in the composite (wt.%).

2.2.3. Processing

Specimens for tensile (ISO-527-1) and flexural testing (ISO- 178) were obtained simultaneously by injection moulding in the family mould (injection moulding machine Euroinj D – 065, Lien Yu Machinery Co., Ltd. Before moulding, the composites were dried for 2 hours at 85 °C in the hopper dryer, connected to the injection moulding machine. Between the change of NFC lots, the injection barrel was purged with neat PP. To ensure the material's purity between the shift of lots, the first 15

Preprints (www.preprints.org) | NOT PEER-REVIEWED | Posted: 11 December 2023 doi:10.20944/preprints202312.0697.v1

parts were discarded before collecting. The injection moulding processing conditions for both the virgin PP and NFC specimens are detailed in Table 2.

Table 2 Injection moulding processing conditions.

Parameter	PPv	NFC
Mould temperature (°C)	40	40
Injection temperature (°C)	230	190
Injection velocity (%)[1]	20	20
Packing time (s)	40	40
Cooling time (s)	35	35

[1] % of the maximum velocity of the injection moulding machine.

2.2.4. Density

Density assessment of the produced composites and neat PP was carried out by a hydrostatic method at room temperature on an A&D GH-252 scale (A&D Company, Limited, Japan), according to ASTM D792. Due to the hygroscopic nature of the NFC specimens, they were dried in the oven with forced ventilation at 50 °C for 48 hours. Following removal of the specimens from the oven, they were put in the desiccator (HC 200 Humidity Control Cabinet by Guangdong SIRUI Optical Co., Ltd) to be brought to laboratory temperature (23 °C) and after that, kept in vacuum-sealed plastic bags before the density measurement. Propanol (2-Propanol of 99.5% purity by Sig-ma Aldridge) was used as an immersion medium to prevent the samples from floating. The propanol density at 25°C is 0.785 g/cm^3 [28]. The sample size was approximately 28 x 12.7 x 3.2mm with a mass of about 1.1 g. The density was assessed by a fivefold replicate for each material lot.

2.2.5. Shrinkage

The composites' dimensional stability was assessed by evaluating the shrinkage parallel to flow according to ASTM D955 with the bar specimen 12.7 by 127 by 3.2 mm (Type A). The length of the mould cavity and the parts were measured with the digital calliper Mitutoyo (precision ±0,01 mm). The average dimensions of five specimens were considered for the shrinkage calculation with Equation 3.

$$S_l = (L_m - L_s) \times \frac{100}{L_m} \quad (3)$$

where: S_l - the shrinkage parallel to flow, %; L_m -the mold dimension parallel to flow, and, L_s - the specimen dimension parallel to flow.

2.2.6. Mechanical properties

X-10kN machine (Shimadzu Scientific Instruments (SSI), Columbia, MD, USA), following the ISO 527-1 and ISO 178 standards, respectively. Ten Type I specimens were subjected to the tensile tests. The experiments were carried out at an ambient temperature in two steps. Initially, the specimens were pulled at a 1 mm/min rate to calculate Young's modulus. In the second stage, a 50 mm/min tensile rate was applied and maintained until the specimens ruptured. The data from this second test was used to determine the yield stress (σ_y) and strain (ε_y), and tensile strength (σ_u) and strain at break (ε_b).

Flexural testing (3-point bending) was performed at a 5 mm/min speed. The beam-type test specimen with the dimensions 127 x 12.7 x 6.35 mm follows the ISO 178 requirement of 20±1 of the length (l) to the thickness (h) ratio. The length span between the supports complies with equation 4.

$$L = (16 \pm 1)h \quad (4)$$

 doi:10.20944/preprints202312.0697.v1

2.2.7. Morphology assessment

Morphological analysis of the fractured surface of the tensile specimens was performed using the Tabletop scanning electron microscope (SEM) HITACHI TM4000. The SEM images were acquired at an accelerating voltage of 15kV. Before imaging, fractured surfaces of the specimens were carbon-coated under vacuum for 60 seconds using the Emitech K950X Carbon Evaporator Sputter to improve the resolution of the micrographs.

SEM micrographs provide the morphology assessment of high accuracy; nevertheless, the area under analysis is limited. To identify the internal microstructure of fibre-reinforced composites and uniformity of the fillers' distribution along the length and through the thickness of the part, micro CT X-ray inspection was used with the images acquired with 14 μm resolution. When exposed to X-ray radiation, the internal structure of a part absorbs it at different percentages, which leads to the fillers' identification. It was accomplished by analysing the fragments of the narrow section (13x3.2x15mm) of the tensile specimens by a Bruker MicroCt Skyscan 1275 microscope (Bruker Corporation, Billerica, MA, USA). A sequence of projections was obtained and reconstructed using NRECON software (Micro Photonics Inc., Allentown, PA, USA). CTAN software was used for the initial 2D/3D image analysis and processing (Bruker Corporation, Billerica, MA, USA). The quantitative data was treated with the open-source public domain software ImageJ 1.54h5 [29].

2.2.8. Chemical composition analysis

Chemical composition analysis was performed with the Energy Dispersive X-ray Spectroscopy (EDS) module of SEM HITACHI's TM4000Plus. EDS was used to determine which chemical elements are present in a sample and estimate their relative abundance. The fractured surface of the tensile specimens was analysed without any additional coating to avoid interference with the element's detection.

2.2.9. Water absorption

A twenty-four-hour immersion test was carried out according to ASTM D570. The water absorption amount (WA) was evaluated by calculating the change in the sample mass with respect to its original mass according to the following Equation 5

$$WA = \frac{(W_t - W_0)}{W_0} 100\% \quad (5)$$

Where: Wt is specimen mass at time t, and Wo is the initial dry mass of the specimen before it is immersed in water. The weighing was carried out within 30 seconds to avoid the error due to desorption. To ensure statistical significance, eight tensile and flexural specimens of each material lot were tested and designated as TS and FS. The initial dry mass was recorded as it follows: before immersion, the specimens were dried in the oven with ventilation for 24 h at 50 °C, cooled in a desiccator, and weighed to the nearest 0.001 g.

3. Results and Discussion

3.1. MFI and physical properties

Polypropylene is one of the lightest polymers with a density below the density of water. Adding the rice husk and olive pit fibres into the PP matrix resulted in a slight increase in melt and solid densities, as shown in Table 3. The density increase is to be expected due to partial collapse of the cellulose cells under high pressure of the injection moulding [14]. A notable reduction in MFI was observed with the addition of rice husk and olive pits. Compared to PPv (Table 3), the melt flow index of PPrh has decreased by about 18% and 38% with an increase in the rice husk content. A similar trend was verified for PPop, where the reduction of MFI was about 21% and 36%. These findings follow the previous research, which attributes this phenomenon to the restriction of the polymer matrix flow due to fibre loading [19]. The fibres effectively act as a thickening agent, reducing the

Preprints (www.preprints.org) | NOT PEER-REVIEWED | Posted: 11 December 2023 doi:10.20944/preprints202312.0697.v1

fluidity of the PP polymer matrix in the vicinity of the fillers. As it can be seen from Table 3, the linear shrinkage of all PPrh and PPop composites in the flow direction is lower than that of neat PP. The lowest shrinkage was observed for PPrh, constituting a 49% decrease for 30% fibre loading compared with PPv. Meanwhile, PPop shows a significant but more moderate reduction of linear shrinkage, up to 30%.

Table 3. Processing and physical properties.

Material	ρs (g/cm³)	ρm(g/cm³)	MFI (g/10min)	MFI ↓*(%)	Shrinkage (%)
PPv	0.824±0.0004	0.722±0.06	12.93±1.50	-	1.31±0.04
PP20%rh	0.888±0.0006	0.781±0.06	10.57±0.64	18.30	0.85±0.01
PP30%rh	0.920±0.0009	0.801±0.05	8.00±0.27	38.20	0.67±0.01
PP20%op	0.891±0.0011	0.813±0.02	10.22±0.29	21.00	1.02±0.03
PP30%op	0.921±0.0011	0.848±0.03	8.23±0.52	36.40	0.91±0.03

*↓- decrease

3.2. Thermal properties

Compared to the virgin PP, the inclusion of the cellulosic fillers into the polymer matrix does not alter the melting and crystallization temperatures of the composites in a statistically significant way, independently of the type and content of the fillers, as shown in Table 4. The enthalpy of fusion was slightly lower for the composites compared to the PPv, which is expected as the amount of PP matrix is lower. However, their crystalline content has increased and was directly correlated with the amount of filler regardless of its type, rising by 23% and 41% for PPrh and 23% and 40% for PPop, respectively. These findings corroborate the data reported in the literature [4,23], attributing the rise in crystal content to the interaction between the filler and PP matrix, promoting the nucleation of PP crystals around the rice husk and olive pit particles. Higher crystallinity indicates the material stiffness [30], suggesting that all tested composites will possess higher elastic modulus and decreased ductility.

Table 4. Thermal properties of the materials.

Material	Tm (°C)	Hm (J/g)	Tc (°C)	Hc (J/g)	X (%)
PPv	149.28±0.40	82.61±2.46	118.61±1.22	76.40±2.23	39.9
PP20%rh	149.26±0.17	80.96±4.68	118.77±0.21	74.60±3.81	48.9
PP30%rh	149.29±0.16	81.57±2.87	118.25±0.22	66.00±2.34	56.3
PP20%op	149.36±0.12	81.50±0.75	119.45 0.10	75.26±0.41	49.2
PP30%op	149.28±0.40	82.61±2.46	118.61±1.22	76.40 ±2.23	56.0

3.3. Mechanical properties

As shown in Table 5, the elastic modulus has increased in all the composites when compared to PPv, with PP20%rh showing the highest increase (35%) and PP30%op exhibiting lesser improvement (22%). The elastic modulus improvement indicates an increase in composites' rigidity, and the difference between the rice husk and olive pit composites may be due to the availability of more area for the rice husk particles to interact with the PP matrix [23,31]. This hypothesis may also explain an improvement in the elastic modulus with the increase in filler content.

The tensile stress at break has also increased, showing a 20% improvement for PPrh independently of the fibre content. The maximum tensile strength of PPop underwent a more moderate increase for PP20%op, while for the higher filler content, there was almost no difference (1%) when compared to neat PP. Finally, the stiffness of the composites was reflected in a significant decrease in elongation at break, with the specimens rupturing at minimal elongation almost immediately after yielding. The deterioration of these properties can be directly linked to the higher content of the lignocellulosic fibres, their non-uniform distribution and insufficient fibre wetting by

Preprints (www.preprints.org) | NOT PEER-REVIEWED | Posted: 11 December 2023 doi:10.20944/preprints202312.0697.v1

the matrix [7]. The reason for the latter may be associated with several functional groups mainly the hydroxyl present at the fibre surface, which in combination with the hydrophobic polymer matrices results in a weak interfacial interaction [32]. Such a phenomenon, in turn, leads to failure under load. Compared to PPv, the worst-case scenarios of ductility loss were 96% for the NFCs with 20% filler content and 97% for the NFCs with 30% filler content, independently of the type. The discussed results corroborate the data shared by other researchers [1,4,14,22].

Table 5. Tensile properties of the materials.

Material	E (MPa)	E↑*(%)	σ_u (MPa)	σ_u ↑*(%)	ε_b (%)	ε_b ↓** (%)
PPv	1020.90±67.00	-	16.28 ±0.74	-	238.2 ±136.3	-
PP20%rh	1377.02±198.2	35	19.65±0.44	20.7	8.55±1.19	96
PP30%rh	1322.58±170.63	30	19.64±0.63	20.6	8.33±1.40	97
PP20%op	1305.80±217.75	28	18.60±0.53	14.3	9.93±1.68	96
PP30%op	1249.57±239.78	22	16.59±0.33	1.0	6.80±1.05	97

*↑ - increase; **↓- decrease

Flexural modulus (E_f) has increased for all the composites, as demonstrated in Table 6. The more pronounced improvement was achieved with a higher concentration of olive pits and rice husk, with the latter showing more potential for enhancing the flexural modulus. Compared with virgin PP, Ef increased by 21 % and 50% for PP20%rh and PP30%rh, respectively. On the other hand, PPop showed more moderate improvement. These results align with the trend reported by the other researchers [3,23]. In the case of flexural strength (σ_f), a slight decrease was observed for most composites (Table 6), particularly notable for PPop. The deterioration of flexural strengths may be attributed to agglomerations of fillers in the matrix, fillers' moisture retention, and weak interlocking between the matrix and filler [1]. Meanwhile, there was one exception to this trend: PP30%rh displayed a slight improvement of about 1.6% in flexural strength, likely due to better rice husk and PP matrix interlocking under compressive stresses.

Table 6. Flexural properties of the materials.

Material	**Ef (MPa)**	**Ef ↑* (%)**	**σf (MPa)**	**σf variation (%)**
PPv	1045.30 ± 42.84	–	30.94 ± 0.94	–
PP20%rh	1263.42 ± 77.10	21	30.29 ± 0.83	- 2.1
PP30%rh	1572.39 ± 66.97	50	31.44 ± 0.88	+ 1.6
PP20%op	1170.49 ± 47.33	12	28.61 ± 0.84	- 7.5
PP30%op	1356.54 ± 95.49	30	28.97 ± 1.44	- 6.4

*↑ - increase

3.4. Morphology assessment

From the SEM micrographs (**Figure** 1) of the fractured cross-sections of the tensile specimens, it is evident that the distribution of fibres in the fractured cross-sections of the tensile specimens is not uniform. Additionally, there are indications of clamping, suggesting poor reinforcement/matrix adhesion and, consequently, lower performance of these composites during tensile tests, as seen in Table 5, with lower values for strain at break and yield strength compared to virgin PP. The non-uniform distribution and clamping were more pronounced in the case of olive pits NFCs (**Figure** 1(c), (d)), where dark areas (voids) resulted from the pulling of fibre from the PP matrix. In contrast, the rice husk NFCs showed a relatively more uniform distribution, particularly in PP30%rh (**Figure** 11b).

Preprints (www.preprints.org) | NOT PEER-REVIEWED | Posted: 11 December 2023 doi:10.20944/preprints202312.0697.v1

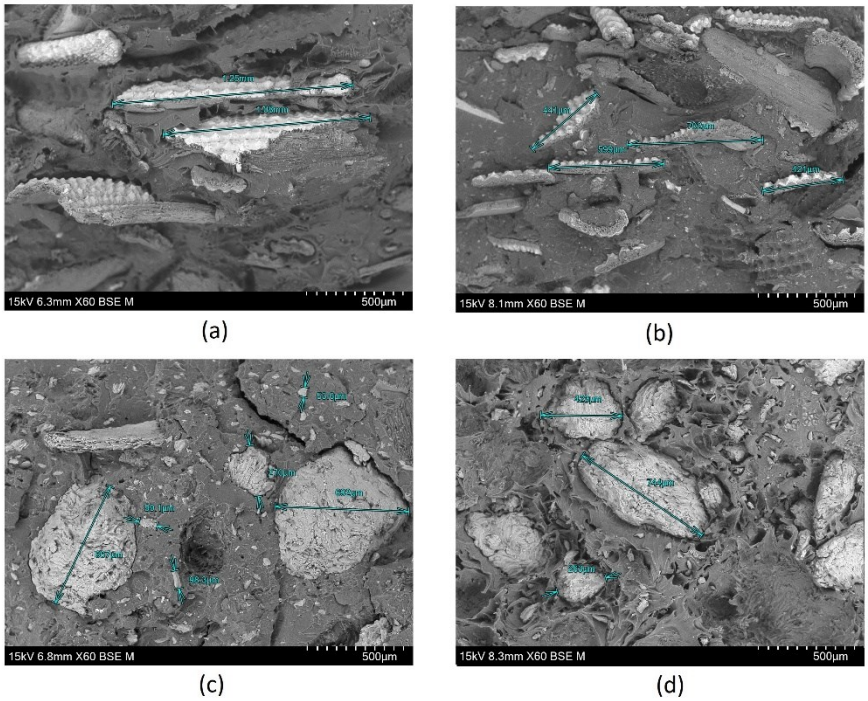

Figure 1. SEM micrographs (60X amplification): (a)PP20%hr, (b)PP30%hr, (c)PP20%op, (d)PP30%op.

Although SEM micrographs provide the morphology assessment of high accuracy, they require destructive preparation of samples and the area under analysis is restricted. Micro CT X-ray inspection is a valuable, non-destructive technique to get an insight into the anisotropy of the fillers' distribution and the granulometry of the incorporated fibres. The fillers are identifiable at the cross sections of the 3D reconstruction of the micro CT scans (**Figure** 2). The non-uniformity of the olive pit particles' distribution through the part thickness is evident in **Figure** 2 (b) and (c), while the distribution of the rice husk fibres (**Figure** 2 (a), (b)) is more uniform. To quantitatively access the granulometry and fillers' distribution through the thickness, three cross-section slices of the area, highlighted in **Figure** 2 (a), were analysed with the Particle analysis module of ImageJ software. The analysed scans were designated further in the text as top, bottom and middle, where the top and bottom are at 0.2 mm from the part´s surface and the middle indicates its centre (**Figure** 3).

The parts here under analysis were obtained by injection moulding as previously referred. As it can be depicted from **Figure** 4 (a), (c), (d), (f), the clustering of the larger olive pit particles, independent of the fillers' load is consistent with the higher viscosity of the polymer melt leading to larger particle retention in the vicinity of the mould wall. The declared maximum granulometry of the olive pit particles before compounding was 0.5mm. However, the histogram of the olive pit particles' size (**Figure** 5) and X-ray diffraction micrographs (**Figure** 4) show a significant variation in the particles' dimensions and many smaller particles. The latter is to be expected. First, it happens during grinding, then due to higher mixing intensity during extrusion and injection moulding and subsequent friction within the particles leading to further size reduction and quantity increase, especially evident for granulometry between 15 and 215 µm equivalent diameter (De) (**Figure** 5). There are more small-size particles in the middle of the part (**Figure** 5), as well as lesser particles' clustering (**Figure** 4 (b) and (d)). Due to lower polymer melt viscosity farther from the mould walls, smaller olive pit particles represent lesser resistance to the polymer flow, gravitating to the hotter middle of the part. The latter was more pronounced for higher 30% olive pit particle content. Nevertheless, there were few particles with granulometry from 500 µm up to 915 µm, possibly due to some olive pit particle grinding and sieving inefficiency. The particles' aggregation and a large amount of the dispersed small-size particles and, hence, larger interface area may explain the inferior mechanical performance of the PPop compared with PPrh (Table 5 and Table 6) due to poor bonding

Preprints (www.preprints.org) | NOT PEER-REVIEWED | Posted: 11 December 2023 doi:10.20944/preprints202312.0697.v1

at the filler–matrix interface region, and a decrease in the stress transfer from the matrix to the filler [12].

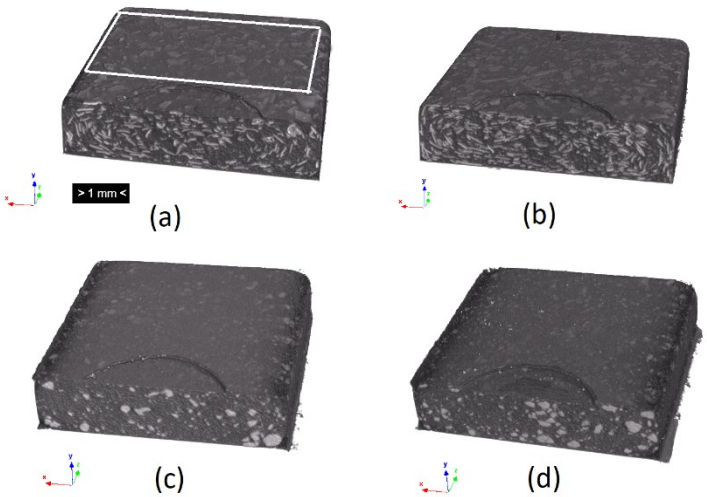

Figure 2. 3D rendering of the micro CT scans: (a)PP20%hr, (b)PP30%hr, (c)PP20%op, (d)PP30%op.

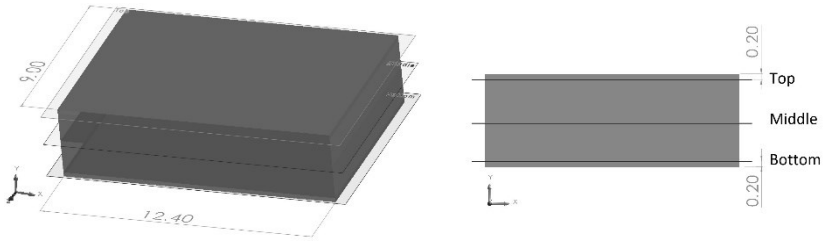

Figure 3. Locations and dimensions of the area under ImageJ analysis.

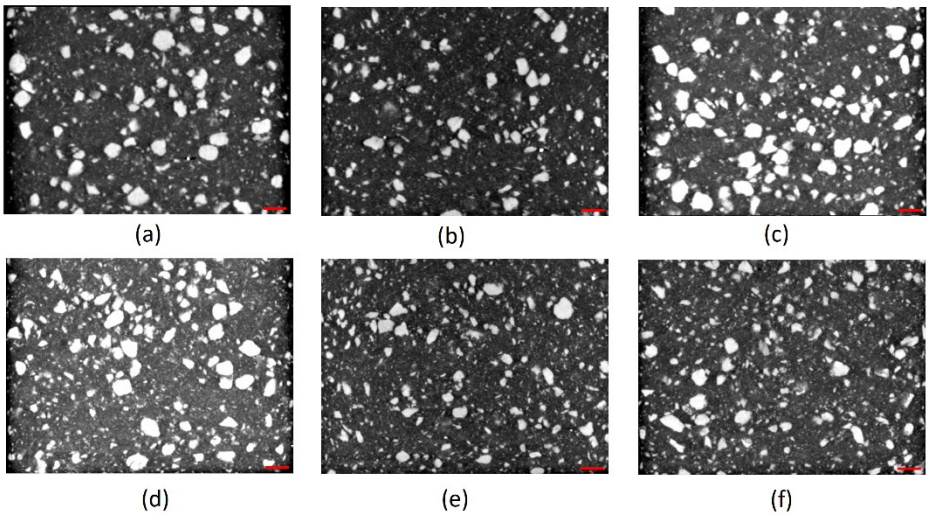

Figure 4. Micro CT scans: PP20%op - (a) Top, (b) Middle, (c) Bottom; and PP30%op - (d) Top, (e) Middle, (f) Bottom. (Scale bar is equal to 1000 μm.).

Preprints (www.preprints.org) | NOT PEER-REVIEWED | Posted: 11 December 2023 doi:10.20944/preprints202312.0697.v1

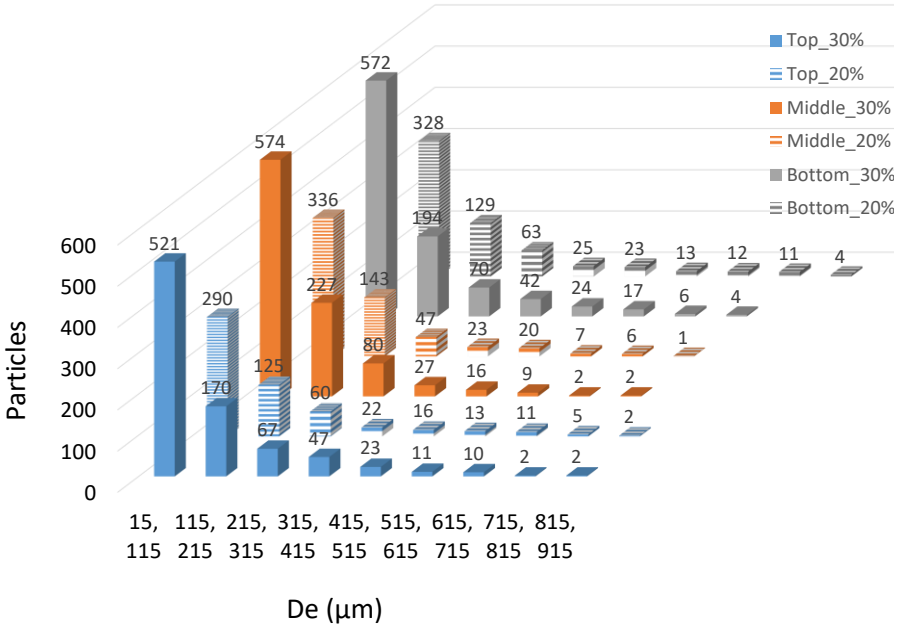

Figure 5. Histogram of the olive pit particles distribution at the top, middle and bottom scan slices.

The rice husk fibres have higher surface-to-area volume ratios and a more irregular shape than the olive pit particles, as shown in **Figure** 6. Thus, their quantitative evaluation was limited to their relative orientation and assessment of the projected area at the different planes through the thickness (**Figure** 7). The rice husk fibres are aligned along the part wall, as shown in **Figure** 6 (a), (c), (d) and (f). The through-thickness projections of the rice husk fibres at the part surface are more extensive than in the middle (**Figure** 6 and **Figure** 7), where the fibres become more randomly oriented (Figure 6 (b), (e)) for both PP20%rh and PP30%rh. The alignment of rice husk fibres along the part wall increased the tensile and flexural moduli (Table 4 and Table 5) and decreased the shrinkage of these composites (Table 2). Stiffer composites are known to be less susceptible to shrinkage [15], so the higher content of the rice husk is directly correlated with higher modulus and inversely correlated with the shrinkage, which decreased from 0.85% for PP20%rh to 0.67% for PP30%rh, as shown in **Figure** 8. The same trend was also verified for PPop.

In addition, for PP30%rh, the rice husk fibres alignment along the mould wall was conducive to higher flexural strength (31.44 MPa) compared to PPv (30.94 MPa), corroborating the conclusions of this material mechanical performance in bending mode. The fibres' alignment near the wall provides better fibre/matrix interlocking under compressive stresses. In addition, mixing during extrusion and injection moulding does not cause a significant reduction of the rice husk fibres size and dispersion of small-size fibres in the PP matrix (**Figure** 1(a), (b)) contrary to the observed for olive pit particles (**Figure** 1 (c), (d). It should be noted that despite the declared maximum particle granulometry of 0.5 mm, many rice husk fibres with much larger dimensions are especially evident at the surface layers, sometimes reaching more than 1 mm in length (**Figure** 6). Besides some inefficiency of sieving, the high aspect ratio and irregular shape of the rice husk fibres may contribute to this more significantly than specified granulometry variation, as the fibres may pass through the sieve oriented perpendicularly to their smaller dimension.

Preprints (www.preprints.org) | NOT PEER-REVIEWED | Posted: 11 December 2023 doi:10.20944/preprints202312.0697.v1

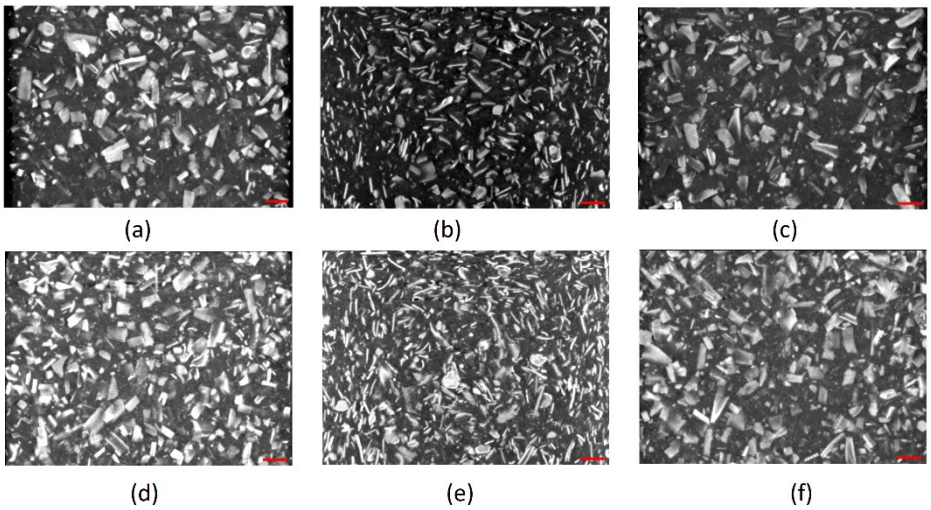

Figure 6. Micro CT scans of PP20%rh: (a) top, (b) middle, (c) bottom PP20%rh; and of PP30%rh (d) top (e) middle, (c) bottom. (Scale bar is equal to 1000 μm.).

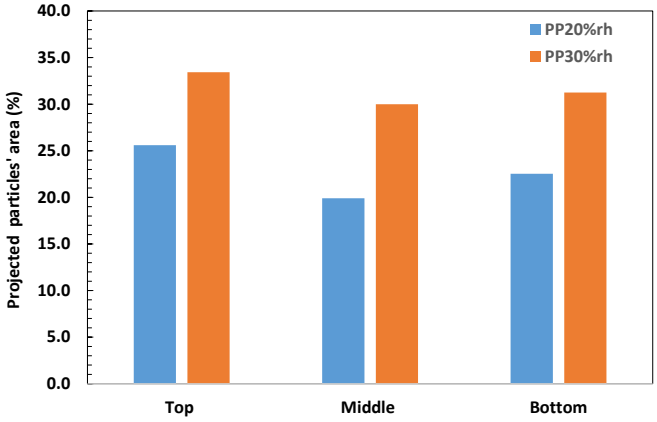

Figure 7. Projected rice husk particles' area at the different part's cross-sections.

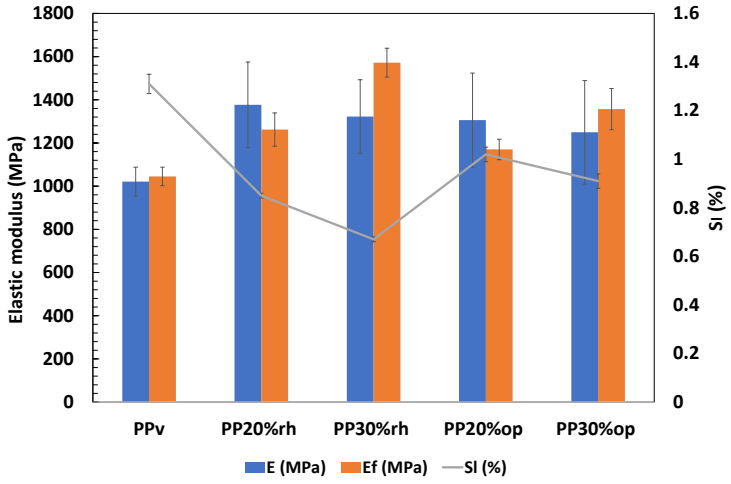

Figure 8. Tensile (E) and flexural (E_f) elastic moduli vs linear shrinkage (S_l) of the composites.

Preprints (www.preprints.org) | NOT PEER-REVIEWED | Posted: 11 December 2023 doi:10.20944/preprints202312.0697.v1

3.5. Chemical composition

Figure 9 and **Figure** 10 show the EDS spectra and the respective zones of the samples under analysis. The samples' chemical composition is listed in Table 7. It should be noted that the equipment used did not detect elements with an atomic number less than 3. X–ray diffraction analysis of PPrh (**Figure** 9 (a) and (b)) shows the presence of carbon, oxygen and silica. The former two elements are present in all lignocellulosic fibres, mainly composed of cellulose, hemicellulose and lignin, and the carbon is also provenient from the PP matrix (**Figure** 9 (c)). The presence of silica is a contribution from the rice husk, especially abundant at the protuberances on the outer and the inner epidermis adjacent to the rice kernel, as has been reported by other authors [3,33].

Considering that the primary molecular compounds of olive pits are mainly hydrogen, carbon and oxygen, in the case of PPop (**Figure** 10), only carbon and oxygen were detected. As shown in **Figure** 9, **Figure** 10 and Table 7. The amount of oxygen has risen with an increase in fibre load, proportionally to a decrease in the amount of carbon. The same observation is valid for silica, which more than doubled with increased rice husk content.

Table 6. Chemical composition of the materials.

Material	Elements' mass (%)		
	C	O	Si
PPv	100	—	—
PP20%rh	82.41	16.17	1.423
PP30%rh	72.06	24.62	3.32
PP20%op	91.03	8.97	—
PP30%op	84.91	15.09	—

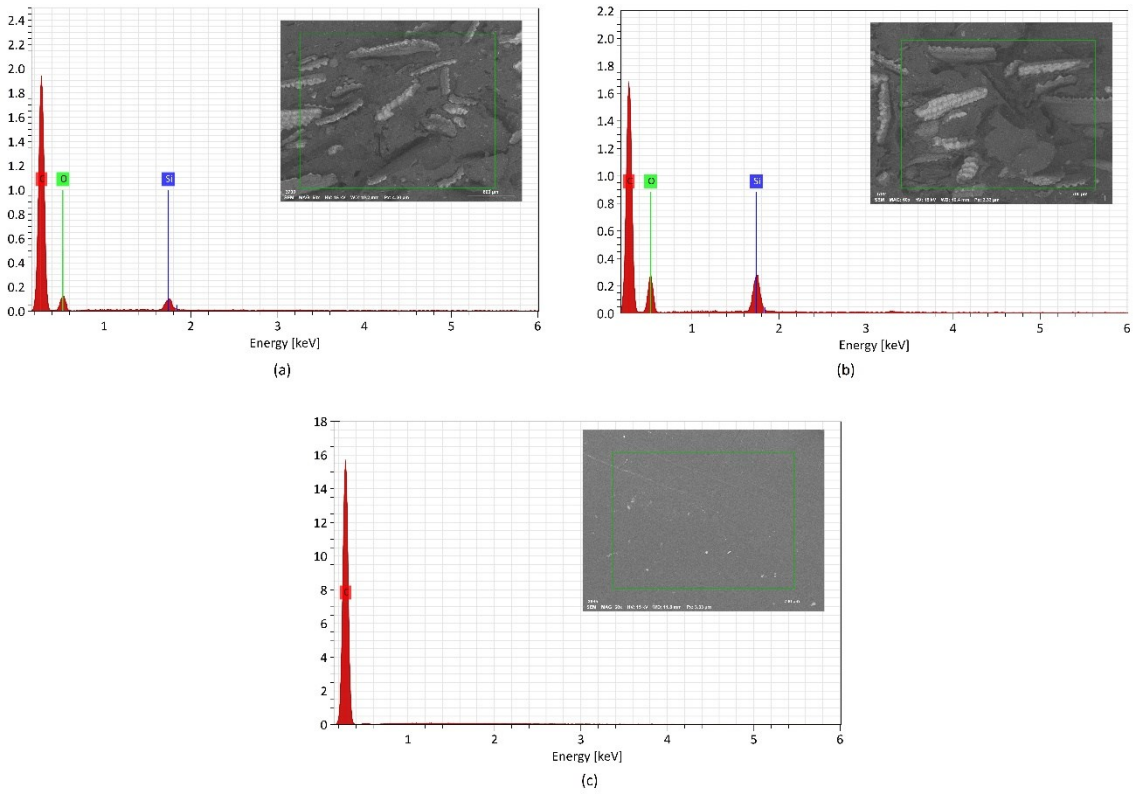

Figure 9. EDS sprectra and the respective zone of the samples under analysis: (a) PP20%rh, (b) PP30%rh, (c) PPv. .

Preprints (www.preprints.org) | NOT PEER-REVIEWED | Posted: 11 December 2023 doi:10.20944/preprints202312.0697.v1

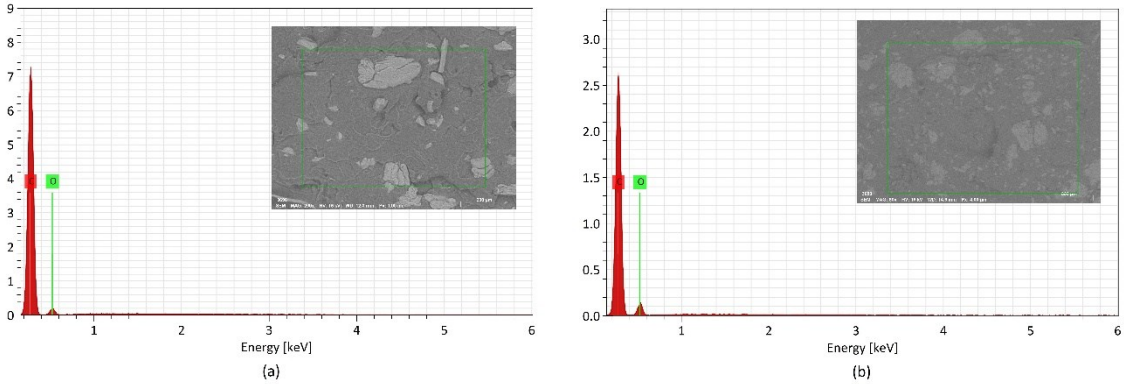

Figure 10. EDS sprectra and the respective zone of the samples under analysis: (a) PP20%op, (b) PP30%op.

3.6. Short-term water absorption

The greatest problem when using lignocellulosic filler in composite materials is its strong sensitivity to water, which is detrimental to their mechanical performance and durability [34]. To explore the potential applicability of the rice husk and olive pit PP-based composites for use in humid conditions, a 24-hour immersion test was carried out, the results of which are shown in Table 7 and **Figure** 11. As it was expected, the water absorption in PPv was less than 0.02% due to its intrinsic hydrophobicity. The inclusion of rice husk and olive pit in the PP matrix leads to a significant increase in water uptake, 0.27% for PPrh and 0.17% for PPop, the value increasing with the filler load independently of its type. It must be mentioned that the thicker specimens (FS) show lower water absorption, as it can be depicted from **Figure** 10, corroborating the data reported in earlier research [35] regarding to the short-term water immersion. For all the composites, the higher water absorption occurs at higher filler loading due to the hydrophilic nature of cellulosic fibres. The presence of hydroxyl (OH) groups between macromolecules of the cellulose, hemicellulose and lignin fibre cell walls promotes the interaction with the water molecules through the hydrogen bonding formation and reduces the interfacial adhesion between the fibre and the matrix [24,34,36–38].

For the rice husk composites, the amount of water absorbed in 24 hours was several times lower than reported by Erdogan et al. [3] for PP rice husk composites with similar fibre load, obtained by compression moulding. The different processing methods may explain this discrepancy, as the injection moulded specimens are more densely packed while solidifying constrained under high pressure and, hence, may be less susceptible to water absorption.

Table 7. Short-term (24h) water absorption.

Specimen type	WA (%)				
	PPv	PP20%rh	PP30%rh	PP20%op	PP30%op
TS	0.015±0.01	0.173±0.03	0.270±0.01	0.12±0.00	0.161±0.01
FS	0.010±0.00	0.109±0.01	0.171±0.01	0.082±0.01	0.121±0.00

Preprints (www.preprints.org) | NOT PEER-REVIEWED | Posted: 11 December 2023 doi:10.20944/preprints202312.0697.v1

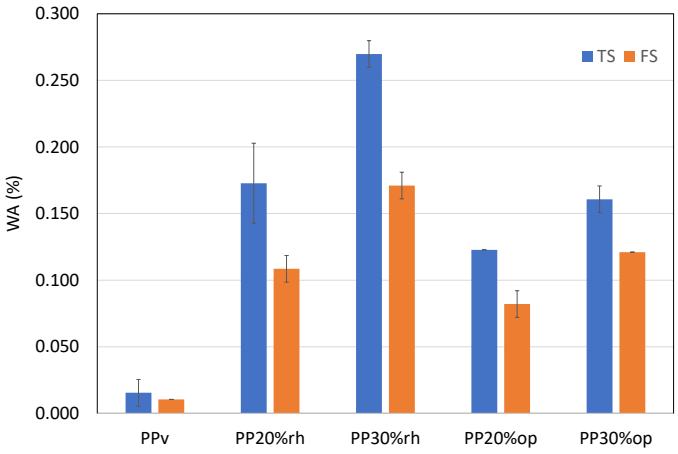

Figure 11. Short-term (24 h) water absorption. .

The higher water absorption PPrh compared to PPop may be attributed to various factors such as filler composition, fibres porosity and their orientation in the PP matrix [36]. Considering that the leading causes of the water absorption in cellulosic fibres are by order of importance hemicellulose, cellulose and lignin [36], the amount of hemicellulose in the rice husk is significantly higher than in the olive pit, as shown in Table 8, promoting the higher water sorption. Moreover, the surface-to-area volume ratios of the rice husk fibres (**Figure** 6) are larger than that of the olive pits (**Figure** 4). A larger interface area of the rice husk particles with the PP matrix and its high porosity ([39] leads to a higher water uptake than that of PPop.

Table 8. Rice husk and olive pit composition.

Filler	Cellulose (%)	Hemicellulose (%)	Lignin (%)	Ref.
Rice husk	42.80	37.20	22.50	[7]
Olive pit	48.62	16.78	33.67	[40]

5. Conclusions

This work has investigated the natural fibre composites with endogenous rice husk and olive pit fibres. These composites were processed at a lower temperature than neat PP to avoid degradation of the cellulosic fibres. Their viscosity has increased with the reinforcement content but remained within the limits of injection moulding processability. The composites have become more rigid than virgin PP as their elastic moduli in tension and bending and the tensile stress at break were improved. The flexural strength of the olive pit composites was inferior to neat PP. In contrast, the rice husk composites showed similar flexural strength at 20% reinforcement and a slight improvement at 30%. The dimensional stability of the latter composites was also superior, with the lower linear shrinkage inversely correlated with superior elastic properties and higher crystallinity. The outstanding performance of the rice husk composites was due to the intrinsic fibre properties: high surface-to-area volume ratio; fibres' alignment near the part walls, providing fibre/matrix interlocking under compressive and tensile stresses, and more uniform distribution as compared with the olive pit composites. However, the same rice husk fibres properties, granting superior mechanical performance, make the respective composites more prone to water absorption.

In conclusion, both composites have the potential to be a viable eco-friendly alternative for virgin synthetic polymer replacement for use indoors without excessive exposure to humid air. The most promising in terms of dimensional stability and superior mechanical properties are the rice husk composites, while the olive pit composites are more resistant to hydrolytic ageing. However, no definite conclusion about using these composites in humid conditions may be currently drawn, after only the short-term water absorption test, requiring the realization of the long-term water absorption test, which is currently in progress.

Author Contributions: Conceptualization, T.Z., J.C. and M.S.A.O.; Data curation, J.C. and T.Z.; Formal analysis, J.C., T.Z. and M.S.A.O.; Funding acquisition, A.C. and M.S.A.O.; Investigation, J.C., T.Z. and M.S.A.O.; Methodology, T.Z. and M.S.A.O.; Project administration, T.Z. and M.S.A.O.; Resources, T.Z., .A.C. and M.S.A.O.; Supervision, T.Z. and M.S.A.O.; Validation, J.C., T.Z. and M.S.A.O.; Writing—original draft, T.Z.; Writing—review & editing, T.Z. and M.S.A.O. All authors have read and agreed to the published version of the manuscript.

Funding: The present study was developed in the scope of the Project "Agenda ILLIANCE" [C644919832-00000035 | Project nº 22], financed by PRR – Plano de Recuperação e Resiliência under the Next Generation EU from the European Union. The present study was supported by TEMA (UIDB/00481/2020 and UIDP/00481/2020)

Informed Consent Statement: Not applicable.

Data Availability Statement: All data generated or analysed during this study are included in this published article.

Acknowledgments: T. Zhiltsova is grateful to Portuguese national funds (OE), through FCT, I.P., in the scope of the framework contract foreseen in the numbers 4, 5, and 6 of Article 23, of the Decree-Law 57/2016, of August 29, changed by Law 57/2017, of July 19).).

Conflicts of Interest: The authors declare no conflict of interest.

References

1. Aridi, N.A.M.; Sapuan, S.M.; Zainudin, E.S.; AL-Oqla, F.M. Mechanical and Morphological Properties of Injection-Molded Rice Husk Polypropylene Composites. *Int. J. Polym. Anal. Charact.* **2016**, *21*, 305–313.
2. Gümüş, B.E.; Yağci, Ö.; Erdoğan, D.C.; Taşdemir, M. Dynamical Mechanical Properties of Polypropylene Composites Filled with Olive Pit Particles. *J. Test. Eval* **2019**, *47*.
3. Erdogan, S.; Huner, U. Physical and Mechanical Properties of PP Composites Based on Different Types of Lignocellulosic Fillers. *J. Wuhan Univ. Technol. Sci. Ed.* **2018**, *33*, 1298–1307.
4. Hidalgo-Salazar, M.A.; Salinas, E. Mechanical, Thermal, Viscoelastic Performance and Product Application of PP-Rice Husk Colombian Biocomposites. *Compos. Part B Eng.* **2019**, *176*, 107135.
5. Made in EU Rice Sustainable EU Rice Available online: https://www.sustainableeurice.eu/sustainable-rice/ (accessed on 3 Dec. 2023).
6. Foundation., F.M. dos S. PORDATA, the Database of Contemporary Portugal Available online: https://www.pordata.pt/en/portugal/olive+production+–+mainland+portugal-3362. (accessed on 25 Nov. 2023).
7. S.D. Genieva, S.Ch. Turmanova, and L.T.V. Utilization of Rice Husks and the Products of Its Thermal Degradation as Fillers in Polymer Composites . In *Cellulose Fibers: Bio- and Nano-Polymer Composites: Green Chemistry and Technology*; Springer Berlin Heidelberg, 2011; pp. 345–377 ISBN 9783642173707.
8. Ray, D. 12 State-of-the-Art Applications of Natural Fiber Composites in the Industry. In *Nat Fiber Compos*; Campilho R.D.S.G., Ed.; Taylor & Francis Group, LLC, 2015; Vol. 5, p. 319.
9. Mallick, P.K. *Polymer Matrix Composites: Processing and Applications*; CRC Press, 2017; ISBN 9781315157252.
10. Berzin, F.; Vergnes, B. Thermoplastic Natural Fiber Based Composites. In *Fiber Reinforced Composites*; Elsevier, 2021; pp. 113–139.
11. Thomas, S.; Jose, S. *Wool Fiber Reinforced Polymer Composites*; The Textile Institute Book Series; Elsevier Science, 2022; ISBN 9780128240571.
12. Malkapuram, R.; Kumar, V.; Negi, Y.S. Recent Development in Natural Fiber Reinforced Polypropylene Composites. *J. Reinf. Plast. Compos.* **2009**, *28*, 1169–1189.
13. Sperling, L.H. *Introduction to Physical Polymer Science*; Wiley-Interscience; Wiley, 2005; ISBN 9780471706069.
14. Burgstaller, C. A Comparison of Processing and Performance for Lignocellulosic Reinforced Polypropylene for Injection Moulding Applications. *Compos. Part B Eng.* **2014**, *67*, 192–198, doi:https://doi.org/10.1016/j.compositesb.2014.07.010.
15. Davis, A.M.; Hanzly, L.E.; DeButts, B.L.; Barone, J.R. Characterization of Dimensional Stability in Flax Fiber Reinforced Polypropylene Composites. *Polym. Compos.* **2019**, *40*, 132–140, doi:https://doi.org/10.1002/pc.24614.
16. Kord, B. Assessment of Long-Term Water Absorption in Natural Fiber Reinforced Thermoplastic Composites Influenced by Filler Rate and Compatibilizer Treatment. *J. Thermoplast. Compos. Mater.* **2013**, *26*, 296–306, doi:10.1177/0892705711423289.
17. Venkatachalaiah, M.A.; Vasudeva Setty, R.N.; Johns, J. Effect of Compatibilizer on the Properties of Areca-Fiber Reinforced Polypropylene Composites. *J. Nat. Fibers* **2022**, *19*, 15261–15275, doi:10.1080/15440478.2022.2121354.
18. Moe Moe; Liao, K. Durability of Bamboo-Glass Fiber Reinforced Polymer Matrix Hybrid Composites. *Compos. Sci. Technol.* **2003**, *63*, 375–387, doi:https://doi.org/10.1016/S0266-3538(02)00225-7.

19. Rosa, S.M.L.; Nachtigall, S.M.B.; Ferreira, C.A. Thermal and Dynamic-Mechanical Characterization of Rice-Husk Filled Polypropylene Composites. *Macromol. Res.* **2009**, *17*, 8–13.
20. Aridi, N.A.M.; Sapuan, S.M.; Zainudin, E.S.; AL-Oqla, F.M. Investigating Morphological and Performance Deterioration of Injection-Molded Rice Husk–Polypropylene Composites Due to Various Liquid Uptakes. *Int. J. Polym. Anal. Charact.* **2016**, *21*, 675–685.
21. Nourbakhsh, A.; Ashori, A.; Tabrizi, A.K. Characterization and Biodegradability of Polypropylene Composites Using Agricultural Residues and Waste Fish. *Compos. Part B Eng.* **2014**, *56*, 279–283.
22. Taşdemir, M. Effects of Olive Pit and Almond Shell Powder on Polypropylene. In Proceedings of the Key Engineering Materials; Trans Tech Publ, 2017; Vol. 733, pp. 65–68.
23. Jurado-Contreras, S.; Navas-Martos, F.J.; Rodríguez-Liébana, J.A.; Moya, A.J.; La Rubia, M.D. Manufacture and Characterization of Recycled Polypropylene and Olive Pits Biocomposites. *Polymers (Basel).* **2022**, *14*, 4206.
24. Chen, R.S.; Ahmad, S.; Gan, S. Characterization of Rice Husk-Incorporated Recycled Thermoplastic Blend Composites. *BioResources* **2016**, *11*, 8470–8482.
25. Kufel, A.; Kuciel, S. Basalt/Wood Hybrid Composites Based on Polypropylene: Morphology, Processing Properties, and Mechanical and Thermal Expansion Performance. *Materials (Basel).* 2019, *12*.
26. Gao, Y.; Hu, W.; Xin, S.; Sun, L. A Review of Applications of CT Imaging on Fiber Reinforced Composites. *J. Compos. Mater.* **2021**, *56*, 133–164, doi:10.1177/00219983211050705.
27. Ehrenstein, G.W.; Riedel, G.; Trawiel, P. *Thermal Analysis of Plastics*; Hanser Publishers: Munchen, Germany, 2004; ISBN 156990362X.
28. Moreau, A.; Sobrino, M.; Zambrano, J.; Segovia, J.J.; Villamañán, M.A.; Carmen Martín, M. Viscosities and Densities of Different Alcohols (1-Propanol, 2-Propanol, 1-Pentanol and 2-Pentanol) at High Pressures. *J. Mol. Liq.* **2021**, *344*, 117744, doi:https://doi.org/10.1016/j.molliq.2021.117744.
29. Schneider, C.A.; Rasband, W.S.; Eliceiri, K.W. NIH Image to ImageJ: 25 Years of Image Analysis. *Nat. Methods* **2012**, *9*, 671–675, doi:10.1038/nmeth.2089.
30. Ismail, N.I.; Ishak, Z.A.M. Effect of Fiber Loading on Mechanical and Water Absorption Capacity of Polylactic Acid/Polyhydroxybutyrate-Co-Hydroxyhexanoate/Kenaf Composite. *IOP Conf. Ser. Mater. Sci. Eng.* **2018**, *368*, 12014, doi:10.1088/1757-899X/368/1/012014.
31. Essabir, H.; El Achaby, M.; Hilali, E.M.; Bouhfid, R.; Qaiss, A. Morphological, Structural, Thermal and Tensile Properties of High Density Polyethylene Composites Reinforced with Treated Argan Nut Shell Particles. *J. Bionic Eng.* **2015**, *12*, 129–141, doi:10.1016/S1672-6529(14)60107-4.
32. Elfaleh, I.; Abbassi, F.; Habibi, M.; Ahmad, F.; Guedri, M.; Nasri, M.; Garnier, C. A Comprehensive Review of Natural Fibers and Their Composites: An Eco-Friendly Alternative to Conventional Materials. *Results Eng.* **2023**, *19*, 101271, doi:https://doi.org/10.1016/j.rineng.2023.101271.
33. Crishnarao, R. V; Godkhindi, M.M. Distribution of Silica in Rice Husks and Its Effect on the Formation of Silicon Carbide. *Ceram. Int.* **1992**, *18*, 243–249.
34. Azwa, Z.N.; Yousif, B.F.; Manalo, A.C.; Karunasena, W. A Review on the Degradability of Polymeric Composites Based on Natural Fibres. *Mater. Des.* **2013**, *47*, 424–442.
35. Zhang, X.; Wang, Y.; Wan, B.; Cai, G.; Qu, Y. Effect of Specimen Thicknesses on Water Absorption and Flexural Strength of CFRP Laminates Subjected to Water or Alkaline Solution Immersion. *Constr. Build. Mater.* **2019**, *208*, 314–325, doi:https://doi.org/10.1016/j.conbuildmat.2019.03.009.
36. Sahu, P.; Gupta, M.K. Water Absorption Behavior of Cellulosic Fibres Polymer Composites: A Review on Its Effects and Remedies. *J. Ind. Text.* **2020**, *51*, 7480S-7512S, doi:10.1177/1528083720974424.
37. Chun, K.S.; Husseinsyah, S.; Syazwani, N.F. Properties of Kapok Husk-Filled Linear Low-Density Polyethylene Ecocomposites: Effect of Polyethylene-Grafted Acrylic Acid. *J. Thermoplast. Compos. Mater.* **2016**, *29*, 1641–1655.
38. Chen, R.S.; Ahmad, S.; Gan, S.; Tarawneh, M.A. High Loading Rice Husk Green Composites: Dimensional Stability, Tensile Behavior and Prediction, and Combustion Properties. *J. Thermoplast. Compos. Mater.* **2020**, *33*, 882–897, doi:10.1177/0892705718815536.
39. Kordi, M.; Farrokhi, N.; Pech-Canul, M.I.; Ahmadikhah, A. Rice Husk at a Glance: From Agro-Industrial to Modern Applications. *Rice Sci.* **2023**, doi:https://doi.org/10.1016/j.rsci.2023.08.005.
40. Abdellah Ali, S.F.; Althobaiti, I.O.; El-Rafey, E.; Gad, E.S. Wooden Polymer Composites of Poly(Vinyl Chloride), Olive Pits Flour, and Precipitated Bio-Calcium Carbonate. *ACS Omega* **2021**, *6*, 23924–23933, doi:10.1021/acsomega.1c02932.